Atmos. Chem. Phys., 5, 1371–1380, 2005
www.atmos-chem-phys.org/acp/5/1371/
SRef-ID: 1680-7324/acp/2005-5-1371
European Geosciences Union

Atmospheric Chemistry and Physics

Nitric Acid Trihydrate (NAT) formation at low NAT supersaturation in Polar Stratospheric Clouds (PSCs)

C. Voigt[1], H. Schlager[1], B. P. Luo[2], A. Dörnbrack[1], A. Roiger[1], P. Stock[1], J. Curtius[3], H. Vössing[3], S. Borrmann[3,4], S. Davies[5], P. Konopka[6], C. Schiller[6], G. Shur[7], and T. Peter[2]

[1]Institut für Physik der Atmosphäre (IPA), DLR Oberpfaffenhofen, 82234 Wessling, Germany
[2]Institut für Atmosphäre und Klima, ETH Zürich, Hönggerberg HPP, CH-8093 Zürich, Switzerland
[3]Institut für Physik der Atmosphäre, Universität Mainz, 55099 Mainz, Germany
[4]Max-Planck-Institut für Chemie, 55128 Mainz, Germany
[5]School of Environment, University of Leeds LS9JT, UK
[6]Forschungszentrum Jülich, ICG-I, 52425 Jülich, Germany
[7]Central aerological observatory, Moscow, reg. 141700, Russia

Received: 8 December 2004 – Published in Atmos. Chem. Phys. Discuss.: 23 December 2004
Revised: 30 March 2005 – Accepted: 15 April 2005 – Published: 8 June 2005

Abstract. A PSC was detected on 6 February 2003 in the Arctic stratosphere by in-situ measurements onboard the high-altitude research aircraft Geophysica. Low number densities ($\sim 10^{-4}\,\mathrm{cm}^{-3}$) of small nitric acid ($HNO_3$) containing particles ($d<6\,\mu$m) were observed at altitudes between 18 and 20 km. Provided the temperatures remain below the NAT equilibrium temperature T_{NAT}, these NAT particles have the potential to grow further and to remove HNO_3 from the stratosphere, thereby enhancing polar ozone loss. Interestingly, the NAT particles formed in less than a day at temperatures just slightly below T_{NAT} ($T>T_{\mathrm{NAT}}-3.1$ K). This unique measurement of PSC formation at extremely low NAT saturation ratios ($S_{\mathrm{NAT}}\lesssim 10$) constrains current NAT nucleation theories. We suggest, that the NAT particles have formed heterogeneously, but for certain not on ice. Conversely, meteoritic particles may be favorable candidates for triggering NAT nucleation at the observed low number densities.

1 Introduction

PSCs form in the winter polar stratosphere at low temperatures by uptake of water and nitric acid into stratospheric sulfate aerosol (Carslaw et al., 1994; Schreiner et al., 1999; Voigt et al., 2000b). At temperatures below the frost point T_{ICE} ($\sim$190 K), ice can nucleate in the supercooled ternary solution (STS) droplets (Koop et al., 2000), and the cloud may become visible as a colourful iridescent ice PSC. PSCs consisting of NAT particles (Voigt et al., 2000a) have been detected in a broad size and number density range. High number densities ($n\gtrsim 10^{-2}\,\mathrm{cm}^{-3}$) of small NAT particles ($d\lesssim 6\,\mu$m) have been measured on small horizontal scales of some hundred square kilometers in cold regions induced by mountain waves (Carslaw et al., 1998; Wirth et al., 1999; Toon et al., 2000; Voigt et al., 2003). These dense PSCs provide sites for heterogeneous reactions that activate halogen species (Peter, 1997) leading to polar ozone destruction. In contrast, low number densities ($n\sim 10^{-4}\,\mathrm{cm}^{-3}$) of large nitric acid containing particles ($10\,\mu\mathrm{m}<d<20\,\mu\mathrm{m}$) have been detected in synoptic-scale PSC fields (Fahey et al., 2001; Northway et al., 2002). Those large NAT particles can denitrify through sedimentation, irreversibly transporting HNO_3 to lower altitudes (Fahey et al., 1990; Mann et al., 2003). Under denitrified conditions, the passivation of active halogen species may be slowed down, thereby enhancing ozone loss.

Here we present measurements and simulations of small ($d<6\,\mu$m) nitric acid containing particles at low particle number density ($n\sim 1.6\times 10^{-4}\,\mathrm{cm}^{-3}$). Provided the temperatures remain below T_{NAT}, these particles can grow to larger sizes, sediment down and remove HNO_3 from the stratosphere, thereby enhancing polar ozone depletion. In contrast to previous measurements, the conditions of particle formation in our case can be precisely constrained: the air parcels have spent less than a day at temperatures 0 to 3.1 K below T_{NAT} or NAT saturation ratios $S_{\mathrm{NAT}}\lesssim 10$. Here, S_{NAT} is the ratio between the HNO_3 partial pressure and the HNO_3 vapor pressure of NAT. An exposure to temperatures below T_{ICE}

Correspondence to: C. Voigt
(christiane.voigt@dlr.de)

can be excluded. How have these NAT particles formed? Besides current NAT nucleation theories, we investigate the potential role of NAT nucleation on meteoritic particles.

2 Arctic winter 2002/2003

The Arctic stratosphere was extremely cold in early winter 2002/2003 with temperatures persistently below T_{NAT} between end of November and mid-January 2003. During this period, PSC formation over large areas influenced the chemical evolution of the polar vortex, led to denitrification of up to 50% and finally provoked a column ozone loss of 20 to 25% by late March (Grooß et al., 2004). The cold phase stopped in mid-January by a major warming associated with a split of the vortex. Stratospheric vortex temperatures were significantly above T_{NAT} for at least two weeks. The vortex gained strength and cooled again in early February, when PSC measurements were taken.

The Vintersol/Euplex project has the aim to characterize ozone loss and PSCs in the Arctic winter 2002/2003. Within the project, a campaign with the high-altitude research aircraft M55 Geophysica and the Falcon took place from 15 January to 14 February 2003 in Kiruna/Sweden. In this period, the Geophysica performed 10 mission flights to altitudes of 20 km.

3 Instrumentation

The Geophysica carried an NO_y chemiluminescence instrument, a Forward Scattering Spectrometer Probe (FSSP-300), a Lidar and a backscatter sonde for particle detection, besides instruments for trace gas and temperature measurements. Here we concentrate on in-situ measurements of PSCs using the NO_y instrument SIOUX (Schlager et al., 2005[1]) and the FSSP (Borrmann et al., 2000).

3.1 NO_y instrument

The NO_y instrument (Schmitt, 2003) is mounted in a pod under the right wing of the Geophysica. Here, NO_y is the sum of reactive nitrogen species (HNO_3, NO, NO_2, N_2O_5, $ClONO_2$, PAN,...), of which HNO_3 is dominant in the stratosphere. The inlet of the NO_y instrument is especially designed for PSC particle measurements. Particulate and gas phase NO_y (total $NO_{y,tot}$) are measured by a forward facing inlet. Calculations following Krämer and Afchine (2004) show that the measured particle number density is enhanced by a size-dependent factor $E(d)$, which reaches 21 for large particles at 70 hPa. In the rear facing inlet, particles larger than the cut-off size of d_{50}=0.2 μm are inertially stripped from the sampled air, so that predominantly gas phase $NO_{y,gas}$ is measured. The heated inlet (35°C) and a subsequent gold converter (300°C) ensure complete evaporation of particulate NO_y and catalytic conversion to NO. Finally the infrared radiation of the reaction NO+O_3 is measured with a chemiluminescence detector. Nitric acid contained in particles ($NO_{y,part}$) is derived by subtracting $NO_{y,gas}$ from $NO_{y,tot}$ and correcting for the particle enhancement.

$$NO_{y,part}=(NO_{y,tot}-NO_{y,gas})/E(d)=\Delta NO_y/E(d) \quad (1)$$

The flow through each inlet is controlled at 1 Nlpm (Normal liter per minute). In the stratosphere (assuming 70 mbar, 200 K and $E(d)$=21 for large particles) this corresponds to an effective particle sampling rate of 8 l s^{-1}. Thus, at a sampling rate of 1 Hz, particle number densities $\lesssim 10^{-4}$ cm^{-3} can be resolved as individual spikes in the total NO_y data assuming that the particles are equally spread in the sampling volume. The NO_y instrument is calibrated before, during and after the flight. The sensitivity of the instrument is 16 000 counts/ppb NO_y. The accuracy of the NO_y data is ±18% for $NO_{y,tot}$ and ±12% for $NO_{y,gas}$. The particle detection limit for $n>10^{-4}$ cm^{-3} is conservatively estimated as 0.3 ppbv Δ NO_y (from the difference between the two channels in periods without particle observation when $T>T_{NAT}$+5 K).

3.2 Optical particle instruments

The modified FSSP (Borrmann et al., 2000) measures the radiation scattered by particles that isokinetically pass through the beam of a HeNe laser. The probe size range is 0.4 to 23 μm in diameter, divided into 30 channels. Due to ambiguities in the Mie scattering coefficient, the particle number density in the channels between 0.7 and 1.9 μm cannot be resolved and hence are detected as a single size interval. The effective sampling volume of $\sim$10 l min^{-1} resulting from the laser geometry restricts the detection to particles with number densities $n\gtrsim 10^{-4}$ cm^{-3} (with 1 min integration time).

Additionally, a Lidar (Mitev et al., 2002) and a backscatter sonde (Adriani et al., 1992) are operated onboard the Geophysica to measure the backscatter and depolarization of particles. The detection limit of the instruments is 3 to 4% volume depolarization at 532 nm.

3.3 Water vapour instrument

Water vapour is measured with the fast in situ stratospheric hygrometer FISH (Schiller et al., 2002) using the Lyman-α photofragment fluorescence technique. The instrument is calibrated before and after the flight. The accuracy of the Lyman-α hygrometer is 5%. In the stratosphere, the precision of a 1 s measurement is 0.15 ppmv H_2O.

[1] Schlager, H., Voigt, C., Volk, M., Davies, S., Carslaw, K., et al.: Observations of denitrification and renitrification in the 2002–2003 Arctic winter stratosphere, Atmos. Chem. Phys. Discuss., in preparation, 2005.

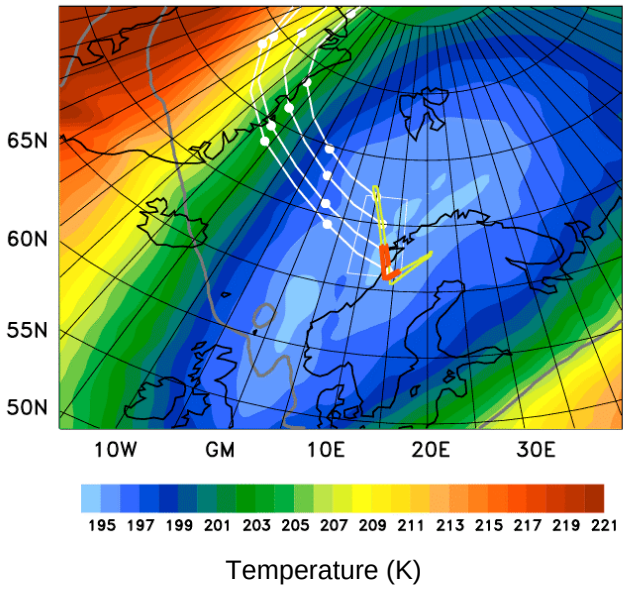

Fig. 1. ECMWF analysed temperature (color coded) at 70 hPa on 6 February 2003 at 12:00 UT. The flight path is marked in yellow and the part of the flight with particle observations is marked by the thick red line. White lines indicate selected air parcel backward trajectories. Each white dot marks a duration of 12 h. The white square indicates the region, in which the trajectories are released. Regions with $T < T_{NAT}$ are inside the blue 197 K contour line. The thick grey line is the vortex edge, defined by a potential vorticity of 3×10^{-6} km^2 kg^{-1} s^{-1}.

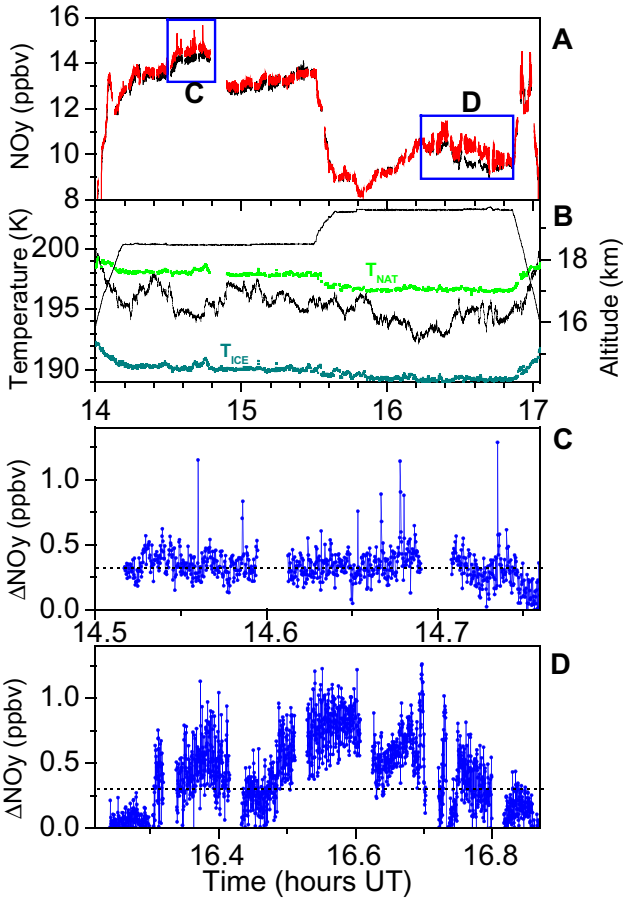

Fig. 2. **(A)** Total NO_y (gas phase plus enhanced particulate NO_y) (red curve) and gas phase NO_y measurements (black curve) versus universal time (UT) on 6 February 2003. Regions with particle observations (red flight segments in Fig. 1) are marked by blue squares. **(B)** Flight altitude (grey), temperature (black), T_{NAT} (green) and T_{ICE} (cyan). The particles were observed at $T > T_{ICE}+4$ K. **(C, D)** Expanded view of particulate reactive nitrogen, ΔNO_y, in regions marked by blue squares in (A). ΔNO_y derives from a subtraction of $NO_{y,tot}$ and $NO_{y,gas}$. Note that ΔNO_y has to be corrected for the particle enhancement, $E(d)$. Particles are indicated by individual peaks in the data (C) and by intensified signal fluctuations (C and D). The dashed black line shows the detection limit for particle NO_y.

3.4 Temperature measurements

The temperature is measured with an accuracy of +0.8/−0.6 K with a Rosemount sensor. Comparisons (M. J. Mahoney, personal communication, 2003) with data from a Microwave Temperature Profiler (MTP) and a PT100 resistance thermometer onboard the Geophysica show that MTP data are on average +0.8 K warmer and the PT100 data are on average −0.1 K colder than the Rosemount data.

4 Detection and identification of a NAT PSC

During a flight from Kiruna over the Atlantic on 6 February 2003, HNO_3 containing particles were observed in the stratosphere by the NO_y instrument. Regions of particle detection are indicated by red thick lines on the flight track in Fig. 1. On the outbound flight leg, individual spikes in the total NO_y time series (Fig. 2) indicate the presence of particles near 14.65 h universal time (UT) inside the polar vortex at an altitude of 18.3 km. On the inbound flight leg, particles were detected as enhanced fluctuations in the total NO_y data near 16.6 h UT at an altitude of 19.5 km. The particles were observed at temperatures between 194.5 and 196 K or 0.8 to 3.1 K below T_{NAT}. Here and in the following, T_{NAT} is calculated from Hanson and Mauersberger (1988) using the water vapour and the gas phase NO_y profiles measured onboard the Geophysica. Thereby we estimate that 80% of the gas phase NO_y is HNO_3.

Under the given stratospheric conditions, NAT is the only nitrogen-containing condensed phase known to be stable. The metastable nitric acid dihydrate (NAD) (Worsnop et al., 1993) can only form at $T \leq T_{NAT} - 2.3$ K. Significant uptake of nitric acid in STS droplets starts 3.5 K below T_{NAT} and the resulting high particle number densities of 10 cm^{-3} can not produce isolated peaks in the NO_y data. Therefore we assume that the measured particles consist of NAT.

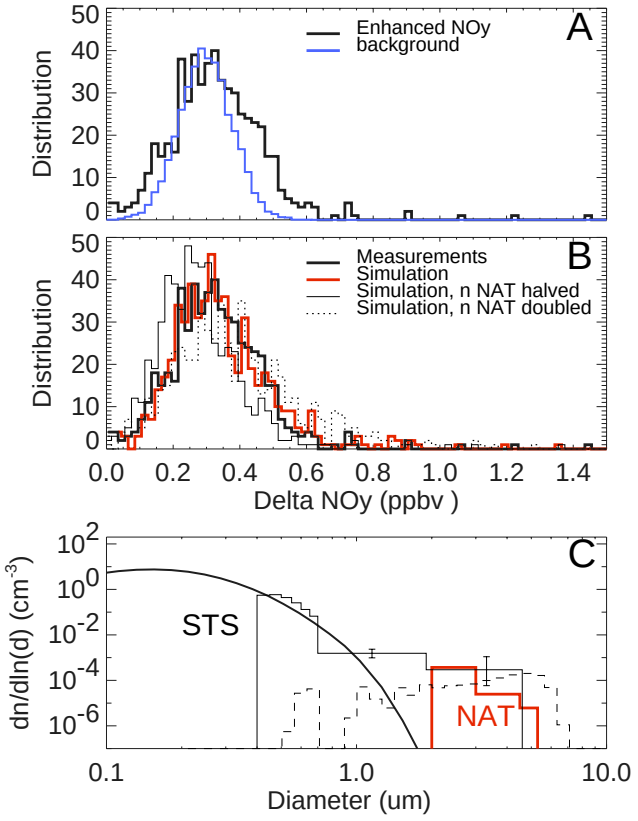

Fig. 3. **(A)** Occurrence histogram of a 600 s long sequence of ΔNO_y data taken in the PSC near 14.65 h UT (black line) compared to the instrument noise near 15.2 h UT (blue line). For better comparison, the instrument background distribution originally centered at 0 has been shifted by +0.3 ppbv on the ΔNO_y axis. **(B)** Fit of the results of the Monte Carlo simulations (red line) to the occurrence histogram of NO_y data taken in the PSC near 14.65 h UT (thick black line). Number density and width of the size classes of NAT particles has been varied in the simulations to fit the occurrence histogram of the NO_y data. Sensitivity studies either halving (thin black line) or doubling the NAT number density (dashed line) lead to significant deteriorations of the fit. **(C)** Particle size distribution at 18.3 km altitude derived from the Monte Carlo simulations of the ΔNO_y data. The particle size distribution consists of a mode of large NAT particles at n=1.6×10^{-4} cm^{-3} (red line). The error in the NAT number density is ± a factor of 2, as derived from the simulations. The small mode (thick black line) consists of STS aerosol with a median diameter of 0.17 μm. The thin black line shows particle size distribution measured by the FSSP. The error bars indicate 96% confidence levels. The dashed line shows the NAT particle size distribution (n=1.5×10^{-4} cm^{-3}) simulated with the DLAPSE model (Carslaw et al., 2002) near the flight track between 410 to 430 K potential temperature in a region of 66–69° latitude north and 12–16° longitude east.

4.1 NAT particle number density and size distribution

We derive particle sizes for the individual peaks in the total NO_y data ascribing their composition to NAT. Modifying an equation from Northway et al. (2002), the particle diameter is:

$$D[\mu m]=4.67 \times (\Delta NO_y[ppbv]/0.9)^{0.33} \quad (2)$$

This assumes 90% of the signal of a NAT particle to be captured during the measurement interval of 1 s, as suggested by the instrument response function. Spikes in the Δ NO_y between 0.6 and 1.3 ppbv (see Fig. 2c) correspond to NAT particles with diameters between 4.1 and 5.4 μm measured between 14.55 and 14.75 h UT. These particles have an average number density n∼6×10^{-6} cm^{-3}, derived using the sampling flow and the particle enhancement factor.

In addition, enhanced fluctuations in the ΔNO_y signal (Fig. 2c and d) indicate the presence of smaller particles with higher number densities ($\gtrsim$10^{-4} cm^{-3}), but these cannot be resolved individually. However, those enhanced fluctuations clearly exceed background instrument noise as shown in Fig. 3a. Therefore we derive the particle number density and size distribution using forward Monte Carlo simulations of the occurrence histogram of the ΔNO_y data. For the simulations, we make an initial guess of the particle size distribution, which consists of a mode of large NAT particles and a second mode of small STS particles. We account for the particle enhancement and assume that the particles evaporate instantly. Further we consider the response time of the instrument, determined by the pumping speed and the volumes of the conversion chamber and the detection chamber. In addition, the instrument background noise has been determined outside of a PSC from the data between 14.8 and 15.5 h UT. We add the simulated ΔNO_y signals stochastically and compare the simulated occurrence histogram with the histogram measured in the cloud between 14.55 and 14.75 h UT. If the agreement is not sufficient, we redefine the size distribution and repeat the steps detailed above.

Good agreement between the measured occurrence histogram of the ΔNO_y data and the simulations (Fig. 3b) is achieved for NAT particles with diameters between 2 and 5.4 μm at n∼1.6×10^{-4} cm^{-3} (red line in Fig. 3c). Those particles contain ∼5 pptv HNO_3. NAT particles with diameters <2 μm cannot be resolved from the data as their signal is masked in slightly enhanced STS aerosol containing ∼0.03 ppbv HNO_3. Sensitivity studies indicate that both doubling or halving the NAT particle number density leads to significant deteriorations of the fit. A similar analysis (not shown here) has been performed for the NAT particles detected on the return flight leg at 19.5 km altitude (Fig. 2d). Those ΔNO_y data can be simulated using NAT particles with diameters between 1 and 3.5 μm and n∼3×10^{-4} cm^{-3} superimposed to slightly enhanced STS aerosol. The error in the NAT particle number density derived from the simulations is ± a factor of 2.

We now compare the particle size distribution to measurements of the optical instruments. We calculate a total backscatter ratio at 532 nm of the observed NAT cloud of 1.001 (compared to 1.0 for air) and a volume depolarization

of 1.42 (compared to 1.4 for air), which lies below the detection limits of the backscatter sonde and the Lidar.

Conversely, the FSSP detected 3 particles with diameters between 1.9 and 4.6 μm near 14.65 h UT besides a small background aerosol mode (thin black line in Fig. 3c). Thus, we use the FSSP data as additional support for the particle size distribution derived from the NO_y instrument, but the low sampling statistics does not allow for a more precise data comparison. In summary, there is a consistency of the particle data derived from the different instruments.

4.2 Extension and vertical structure of the NAT cloud

On 6 February 2003, a NAT PSC is measured inside the polar vortex above the Atlantic ocean near the Norwegian coast. At an altitude of 18.3 km (420 K), a low number density ($\sim 1.6\times10^{-4}$ cm^{-3}) of NAT particles with $d<6\,\mu$m are detected over a distance of 140 km. Above these particles at 19.5 km (440 K), almost twice the number density of smaller NAT particles ($d<3.5\,\mu$m) are measured over a distance of 250 km, probably in the same cloud. Lidar measurements onboard the Geophysica suggest that the NAT particles were measured in an optically thin NAT cloud.

4.3 Simulations of NAT particle growth

We calculate how large a NAT particle can grow at different temperatures assuming 5 ppmv water and 10 ppbv nitric acid in the gas phase and taking into account the uptake of nitric acid into STS aerosol (Fig. 4). Ice particles only exist at 7.5 K below T_{NAT}, and therefore HNO_3 uptake on ice is not important for this study. HNO_3 depletion due to uptake in NAT has also been neglected regarding the low HNO_3 content of the observed NAT particles.

A NAT particle can grow to a diameter of 6 μm, if temperatures remain 2 K below T_{NAT} for 16 h. At temperatures few K above the ice frost point, the NAT particle growth is reduced due to HNO_3 uptake into ternary solution particles. The slower growth of the particles to the same size at these extremely low temperatures reflects the fact that it takes time to release the HNO_3 from the metastable STS droplets, to establish its diffusive transport through the gas phase and finally its uptake by the NAT particle in a Bergeron-Findeisen-like process.

Further, we performed a vortex wide simulation of NAT particles using the DLAPSE model, which couples a Lagrangian NAT particle growth and sedimentation scheme to the three-dimensional chemistry transport model SLIMCAT (Carslaw et al., 2002). We use a NAT nucleation rate of $J_{NAT}=1.15\times10^{-5}$ cm^{-3} air h^{-1} and we improve the model sampling statistics for low particle number densities in this study. The model shows the existence of 1.5×10^{-4} cm^{-3} NAT particles with diamaters between 1 and 7 μm near the flight track on 6 February 2003 in good agreement with the observations. Figure 3c (dashed line) shows the modelled

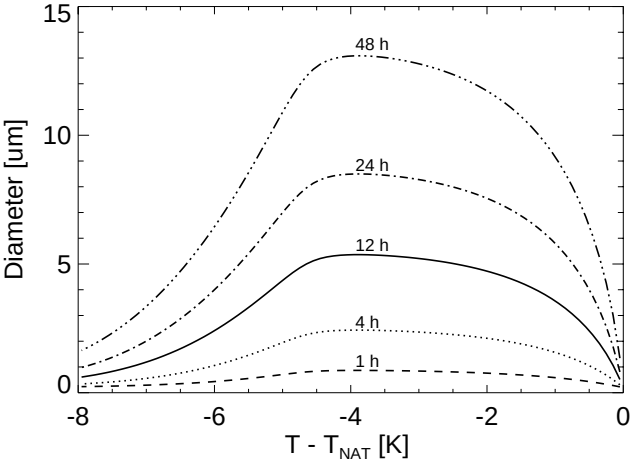

Fig. 4. Box model calculation of NAT particle growth for 10 ppbv total HNO_3 and 5 ppmv H_2O at 50 hPa as a function of the temperature difference to T_{NAT}. The black lines show NAT particle diameters for different growth times between 1 h and 2 days. The deceleration of NAT growth at low temperatures results from gas phase depletion of nitric acid due to uptake in ternary solution droplets.

NAT particle size distribution in a region of 66–69° N and 12–16° E between 410 and 430 K. At higher altitudes between 430 and 450 K, the existence of smaller NAT particles with higher number densities is simulated with the DLAPSE model in qualitative agreement with the observations.

We note that the DLAPSE model simulates NAT particles in a slightly larger area than observed and also the shape of the size distributions differs from the observations. This may result from different spacial resolutions of the measurements and the simulations. Further the simulation of NAT formation at a constant rate at temperatures below T_{NAT} is a simplified approach. In the real atmosphere, the particle nucleation process presumably depends on temperature, NAT supersaturation and composition of the air masses. Assuming an increase in the NAT nucleation rate with NAT supersaturation might explain discrepancies in the shape of the size distribution and the region of particle observation.

4.4 Comparison with other PSC measurements

During the Euplex campaign, thin STS PSCs containing up to 0.5 ppbv nitric acid were detected in mountain waves on two flights (Lowe et al., 2005[2]). Although temperatures below T_{NAT} were encountered on 4 flights, trajectory temperatures were less than 8 h below T_{NAT} in those cases except on 6 February. NAT particles can grow to diameters of 3.3 μm in 8 h, which is near the detection limit of the NO_y

[2]Lowe, D., MacKenzie, A. R., Schlager, H., et al.: Liquid particle composition and heterogeneous reactions in a mountain wave polar stratospheric cloud, Atmos. Chem. Phys. Discuss., in preparation, 2005.

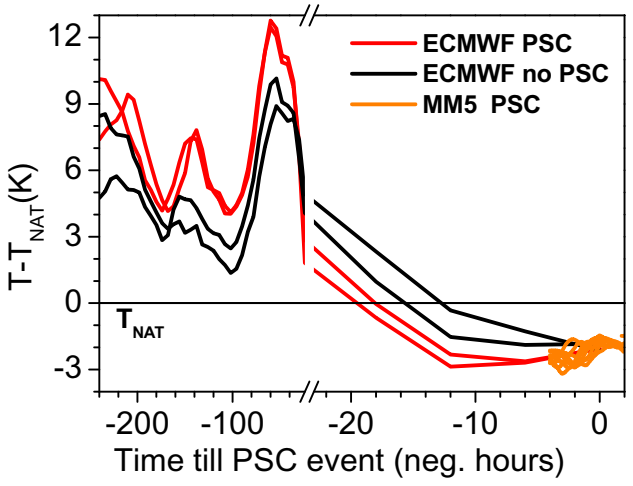

Fig. 5. $T-T_{\mathrm{NAT}}$ along 3-D backward trajectories based on 6-h T511/L60 ECMWF operational analysis (red and black lines) and trajectories calculated with the mesoscale MM5 model (Dörnbrack et al., 1999) (orange lines). Black lines are trajectories ending on the flight path outside of PSC observations and red and orange lines are trajectories ending in the PSC observations on the Geophysica flight path.

instrument. Nitric acid containing particles with $d>3.3\,\mu$m were detected only on 6 February 2003.

We now compare our measurements to previous PSC observations. In winter 1999/2000, NO_y containing particles with low number densities ($n\sim10^{-4}\,\mathrm{cm}^{-3}$) but larger diameters ($10\,\mu\mathrm{m}<d<20\,\mu\mathrm{m}$) have been detected in the Arctic stratosphere (Fahey et al., 2001; Northway et al., 2002). These particles could also be inferred from satellite extinction data (Poole et al., 2003). In addition, small NAT particles ($d<6\,\mu$m) with higher number densities (few times $10^{-3}\,\mathrm{cm}^{-3}$) have been detected during several balloon flights in Arctic mountain waves (Deshler et al., 2003; Schreiner et al., 2003) or during synoptic cooling (Larsen et al., 2004).

Measurements of low number densities ($n\sim10^{-4}\,\mathrm{cm}^{-3}$) of small NAT particles ($d<6\,\mu$m) as observed in the present case have not been reported so far, as they are not detectable with most instruments. This does not only underline the unique capability of the NO_y instrumentation, it is also the reason for the paucity of such measurements. These NAT particles are not necessarily rare, but hard to detect.

5 Trajectory analysis

The particle measurements on 6 February 2003 took place in a short period with temperatures for a few days slightly below T_{NAT} in the lower Arctic stratosphere. Therefore we perform an accurate trajectory analysis to gain new insights in NAT formation at threshold PSC formation conditions.

We calculated trajectories based on ECMWF analysis ending in a wider region around the flight track indicated by the white square in Fig. 1. The back-trajectories were started on a grid in steps of 0.5° latitude and longitude and at altitudes of 70 hPa (pressure altitude on the outbound flight leg), 55 hPa (pressure altitude on the return flight leg) and 50 hPa. The difference between the trajectory temperatures at 70 hPa and T_{NAT} is shown in Fig. 5. Selected trajectories ending on the flight track in regions with NAT particle observations are shown as red lines, trajectories ending in cloud free air are marked in black. The geographical location of the trajectories is shown in Fig. 1.

In the time period of one day, the descent rate of particles with diameters $<5\,\mu$m due to gravitational settling is slow ($\leq$200 m/day) and comparable to the descent rate air by diabatic cooling ($\sim$100 m/day). Therefore, we consider the calculated air parcel temperature as an approximated temperature history of the NAT particles.

The trajectory temperatures were above T_{NAT} for more than a week before they decrease below $T_{\mathrm{NAT}}\sim$20 h before particle detection. The absolute temperature minimum reached by any of the trajectories is $T_{\mathrm{NAT}}-3.1$ K or $T_{\mathrm{ICE}}+4.4$ K. This conclusion holds even when allowing for mesoscale temperature fluctuations related to gravity waves above the Scandinavian Alps (orange lines in Fig. 5), which were calculated using the mesoscale MM-5 model (Dörnbrack et al., 1999). For the return flight leg at 55 hPa and also at the 50 hPa level, the trajectory temperatures (not shown here) were even higher. They were less than 19 h below T_{NAT} reaching minimum values of $T_{\mathrm{NAT}}-2.2$ K. This meteorological situation with low atmospheric temperature variability allows us to constrain temperatures for particle formation to $T>T_{\mathrm{NAT}}-3.1$ K or $S_{\mathrm{NAT}}\lesssim10$.

6 NAT formation

Given that the trajectory temperatures remain 20 h below T_{NAT}, we derive an average NAT nucleation rate $J_{\mathrm{NAT}}=8\times10^{-6}\,\mathrm{cm}^{-3}$ air h^{-1} at temperatures below T_{NAT} to explain the measured particle number density of $1.6\times10^{-4}\,\mathrm{cm}^{-3}$.

A NAT nucleation rate of similar magnitude ($1.15\times10^{-5}\,\mathrm{cm}^{-3}$ air h^{-1}) has been derived from MLS observations in the winters 1994/1995, 1996/1997 and 1999/2000 (Davies et al., 2005). A factor of 4 lower NAT nucleation rate has been determined from ER-2 measurements in the Arctic winter 1999/2000 (Fahey et al., 2001; Carslaw et al., 2002).

Different studies exist for the Arctic winter 2002/2003. A higher NAT nucleation rate ($2.5\times10^{-5}\,\mathrm{cm}^{-3}$ air h^{-1}) has been derived from balloon-borne measurements of NAT PSCs (Larsen et al., 2004) in December 2002. DLAPSE simulations show that the winter 2002/2003 denitrification can well be modelled using a nucleation rate of

$1.15\times10^{-5}\,\mathrm{cm}^{-3}$ air h^{-1} (S. Davies, personal communication, 2004). Grooß et al. (2004) investigate the effect of different nucleation rates. They find that a nucleation rate of $8\times10^{-6}\,\mathrm{cm}^{-3}$ air h^{-1}, as derived from our study, best fits the denitrification in the Arctic winter 2002/2003. In all studies detailed above, the average NAT nucleation rate varies by less than an order of magnitude in 4 different winters.

As NAT nucleation is a subject of current scientific debate (Tolbert and Toon, 2001), we use the NAT cloud observation in this unique situation at threshold NAT formation conditions ($S_{\mathrm{NAT}}\lesssim10$) to discuss different theories of NAT particle formation.

6.1 Homogeneous NAT nucleation

Homogeneous nucleation rates of NAT/NAD in ternary solutions have been determined from laboratory experiments (Koop et al., 1995, 1997; Salcedo et al., 2001; Knopf et al., 2002). Other laboratory studies with binary solutions show that the metastable NAD may form as the precursor of NAT, later performing a transition to NAT (Worsnop et al., 1993). The result of our trajectory analysis ($T>T_{\mathrm{NAT}}-3.1\,\mathrm{K}$) strongly suggests, that those particle are neither composed of NAD nor have nucleated on NAD. Another analysis of laboratory experiments suggests that the nucleation of solids occurs on the surface rather than in the volume of liquid particles (Tabazadeh et al., 2002). At $S_{\mathrm{NAT}}\lesssim10$, the nucleation rates given in each of those laboratory studies cited above are by more than 2 orders of magnitude too low to explain the present observations.

6.2 NAT sedimentation from higher altitudes

The trajectories at the observational levels and above (70, 55 and 50 hPa) show temperatures more than 5 K above T_{NAT} for more than a week before decreasing below T_{NAT} approximately one day prior to the measurements (Fig. 5). A 16 μm NAT particle evaporates within 8 h at 3 K above T_{NAT}. Therefore previously formed NAT particles would not survive such a warm period. The air must be NAT free on 5 February 2003 and the measured NAT particles have formed in less than a day. In one day, NAT particles can grow to a maximum diameter of 8 μm and sediment less than 500 m, therefore the sampled particles have formed in a small altitude range of few 100 m.

The Micro-Lidar (Mitev et al., 2002) onboard the Geophysica measures no significant increase of depolarization and backscatter ratios at 532 nm above the background aerosol level in the region 5 km above and below the flight track. Thus, the particles were measured in an optically thin NAT cloud and not below a dense NAT cloud.

Additionally, the dynamical activity in the stratosphere due to mesoscale wave activity was low on 6 February with maximum temperature deviations of the mesoscale trajectories of ±0.7 K from ECMWF trajectories (Fig. 5). The minimum trajectory temperatures are reached above the Atlantic ocean, where mesoscale wave activity is expected to be small.

Combined, those arguments suggest that NAT sedimentation out of mountain wave clouds (Füglistaler et al., 2002; Dhaniyala et al., 2002) can be ruled out.

6.3 Heterogeneous NAT nucleation on ice

Lidar and in situ measurements in mountain wave PSCs (Carslaw et al., 1998; Wirth et al., 1999; Voigt et al., 2000a) as well as model simulations (Luo et al., 2003) show that NAT can nucleate on ice. However, on 6 February 2003 NAT nucleation on ice can be excluded, because the synoptic ECMWF trajectories and even the mesoscale MM5 trajectories were by more than 4 K above the T_{ICE}, thus significantly too high for ice formation. The present measurements convincingly demand a NAT formation mechanism above the ice frost point, which has also been claimed in recent model studies (Carslaw et al., 2002; Drdla et al., 2003) or PSC observations at $S_{\mathrm{NAT}}\sim30$ (Larsen et al., 2004).

6.4 NAT nucleation on meteoritic particles

Neither homogeneous NAT nucleation nor NAT nucleation on ice can explain the present observations. Therefore other nuclei must be available in the stratosphere, on which NAT can nucleate either by heterogeneous immersion nucleation (the nuclei are immersed in the preexisting STS droplets) or by heterogeneous deposition nucleation (nucleation of NAT directly from the gas phase). One potentially important, ubiquitous kind of nuclei are meteoritic smoke particles. Most (60%) of the meteoritic mass influx in the atmosphere of $8\text{–}30\times10^{6}$ kg per year ablates at altitudes above 75 km due to frictional heating in the atmosphere (Cziczo et al., 2001). Model studies indicate that the ablation products recondense and coagulate in the mesosphere forming nanometer-sized smoke particles (Hunten et al., 1980). Following atmospheric circulation and sedimentation, most of the meteoritic particles are likely to enter the stratosphere over the winter pole. The meteoritic particles traverse the stratosphere in more than a year, during which they may become well-mixed, homogenized and partly incorporated into the stratospheric sulfate aerosol (Cziczo et al., 2001). Mass spectrometric measurements detected meteoritic inclusions in half of the stratospheric particles (Murphy et al., 1998; Cziczo et al., 2001). Curtius et al. (2005)[3] report in a detailed study that the fraction of stratospheric particles containing detectable amounts of involatile material (probably of meteoritic origin) increases markedly inside the polar vortex

[3]Curtius, J., Weigel, R., Vössing, H.-J., Wernli, H., Werner, A., et al.: Observations of meteoritic material and implications for aerosol nucleation in the winter Arctic lower stratosphere from in situ particle measurements, Atmos. Chem. Phys. Discuss., in preparation, 2005.

to ∼70%. Meteoritic material has also been found in cirrus clouds near the tropopause (Cziczo et al., 2004).

We estimate the meteoritic surface area by assuming that half of the stratospheric sulfate aerosol with a typical lognormal size distribution (d_m=0.15 μm, σ=1.65, n=10 cm^{-3}) (Deshler et al., 2003) and a density of 1.72 g cm^{-3} (72 wt% sulfuric acid/water solution) contains 0.75 wt% meteoritic iron (Cziczo et al., 2001). Further we assume that meteoritic material contains 20 wt% iron (ϱ=3 g cm^{-3}, Cziczo et al., 2001). Then we derive a meteoritic surface area density A_{min}=0.05 μm^2 cm^{-3} for a lognormal size distribution of meteoritic particles with a mean diameter of 0.044 μm using the Hatch-Chaote-Equation (Hinds, 1999). For comparison, the volume of the meteoritic material is <3% of the sulfate aerosol. Model simulations of continuously coagulating spherical meteoritic smoke particles derive a meteoritic surface area density of similar magnitude (∼0.1 μm^2 cm^{-3}, Hunten et al., 1980). The meteoritic surface area may be underestimated by up to two orders of magnitude, because the meteoritic smoke particles are expected to form loosely packed agglomerations and not spheres (0.05–5.0 μm^2 cm^{-3}) (Cziczo et al., 2001; Hunten et al., 1980). Additionally, micro-meteorites, variations in the extraterrestrial meteoritic flux or seasonal/interannual changes in the stratospheric circulation, including the formation of the polar vortex, can lead to inhomogeneities and variations of the meteoritic surface area.

Laboratory measurements by Bogdan et al. (2003) on smoked silica particles, considered as representatives for meteoritic smoke particles, show that fine silica particles can induce heterogeneous freezing of NAT in binary solutions at temperatures above the ice frost point. Further, heterogeneous nucleation of ternary solutions on micrometeorites has been investigated calorimetrically by Biermann et al. (1996). They found that the presence of meteoritic material accelerates the freezing of supercooled ternary solutions. Further, they determined an upper limit of the heterogeneous NAT nucleation rate per surface area of meteoritic material of j_{max}=1.4×10^{-4} μm^{-2} h^{-1} at S_{NAT}>25.

By combining the laboratory data and in situ measurements of meteoritic particles, we obtain a very rough estimate for the NAT nucleation rate on meteoritic particles of $J_{\mathrm{NAT}}=j_{max}\times A_{min}$=7×10^{-6} cm^{-3} h^{-1} in the stratosphere. Although this neatly coincides with the experimentally observed value (8×10^{-6} cm^{-3} air h^{-1}), we note that an estimate based on a product of an upper and a lower limit (for the rate and for the surface area, respectively) needs to be treated with caution. Since the heterogeneous nucleation of NAT has not been investigated at NAT saturation ratios as low as observed ($S_{\mathrm{NAT}}\lesssim$10), there is an additional gulf of uncertainty in this result. Conversely, the investigation of Biermann and coworkers refers only to immersion nucleation, while deposition nucleation remains another possible and yet untested pathway for NAT nucleation.

In summary, contrasting to the conclusions of Biermann et al. (1996), who aimed at excluding meteoritic material as responsible for dense (n>10^{-2} cm^{-3}) NAT clouds, the discovery of large singular NAT particles ("NAT rocks", n∼10^{-4} cm^{-3}) makes meteoritic smoke particles favorable candidates for triggering NAT nucleation.

6.5 Discussion

Given the present knowledge, NAT nucleation on meteoritic particles can be regarded as a possible pathway for the formation of solid polar stratospheric cloud particles at low number densities. Assuming temperatures below T_{NAT} for more than 3 days, the estimated rate can produce NAT particle number densities of few times 10^{-4} cm^{-3} as observed by Fahey et al. (2001).

Recent laboratory experiments (Mangold et al., 2005) of ice nucleation on mineral dust show that even the same sort of test dust has varying ice nucleation capabilities and the ice nucleation occurs over a range of ice supersaturations. A similar behavior could be expected for NAT formation on meteoritic particles in the stratosphere.

7 Conclusions

Low number densities (n∼1.6×10^{-4} cm^{-3}) of NAT particles with diameters d<6 μm were detected by in-situ instruments onboard the Geophysica in the Arctic polar stratosphere in winter 2002/2003. In contrast to previous observations, those particles have formed in less than a day at high temperatures ($T>T_{\mathrm{NAT}}-3.1$ K) thus very low NAT supersaturations ($S_{\mathrm{NAT}}\lesssim$10), which until recently has not been considered likely to happen. NAT nucleation at temperatures so close to T_{NAT} increases the time scales and regions of PSC occurrence, which in turn may lead to more efficient denitrification and thus to enhanced polar ozone loss.

Given the scarcity of data, we estimate here a constant average NAT nucleation rate J_{NAT}=8×10^{-6} cm^{-3} air h^{-1} for the temperature range $T_{\mathrm{NAT}}\geq T>T_{\mathrm{NAT}}-3.1$ K. A dependence on temperature or NAT supersaturation can not be determined from these data. Also, the NAT nucleation rate may vary from year to year or during the course of a winter. For the late Arctic winter 2002/2003 calculations with the NAT nucleation rate derived in the present study reasonably reproduce our observations of NAT particle number density, size distribution and also of denitrification (Grooß et al., 2004).

We show that NAT nucleation on ubiquitous meteoritic smoke particles may present a plausible pathway for solid particle formation at temperatures above the ice frost point. However, the detailed mechanism and the spatial and temporal variation of the meteoritic smoke particles as well as the temperature dependence of the NAT nucleation rate remain a challenge for future laboratory and field studies.

Acknowledgements. We thank the Geophysica crew, F. Stroh for excellent project co-ordination, J.-U. Grooß for trajectory data, M. Mahoney for temperature comparisons, R. Weigel for CN counter data, F. Cairo and R. Matthey for data from optical instruments, K. Carslaw and M. Krämer for helpful discussions. We thank the European Centre for Medium-range Weather Forecasts and MeteoSwiss for meteorological data. This work has been funded by the European Community and the Swiss BBW under the contracts EVK2-2001-00084-EuPLEx and EVK-2000-00077-MAPSCORE.

Edited by: K. S. Carslaw

References

Adriani, A., Deshler, T., Gobbi, G. P., et al.: Polar stratospheric clouds over McMurdo, Antarctica, during the 1991 spring: Lidar and particle counter measurements, Geophys. Res. Lett., 19(17), 1755–1758, doi:10.1029/92GL01941, 1992.

Biermann, U. M., Presper, T., Koop, T., et al.: The Unsuitability of Meteoritic and Other Nuclei for Polar Stratospheric Cloud Freezing, Geophys. Res. Lett., 23, 1693–1696, 1996.

Bogdan, A., Molina, M. J., Kulmala, M., MacKenzie, A. R., and Laaksonen, A.: Study of finely divided aqueous systems as an aid to understanding the formation mechanism of polar stratospheric clouds: Case of HNO3/H2O and H2SO4/H2O systems, J. Geophys. Res., 108(D10), 4302–4312, doi:10.1029/2002JD002605, 2003.

Borrmann, S., Thomas, A., Rudakov, V., et al.: In-situ aerosol measurements in the northern hemispheric stratosphere of the 1996/7 winter on the Russian M-55 Geophysika high altitude research aircraft, Tellus, 52B, 1088–1103, 2000.

Carslaw, K. S., Luo, B. P., Clegg, S., et al.: Stratospheric aerosol growth and HNO_3 gas phase depletion from coupled HNO_3 and water uptake by liquid particles, Geophys. Res. Lett., 21, 2479–2482, 1994.

Carslaw, K. S., Wirth, M., Tsias, A., et al.: Particle Microphysics and Chemistry in Remotely Observed Mountain Polar Stratospheric Clouds, J. Geophys. Res., 103, 5785–5796, 1998.

Carslaw, K. S., Peter, T., and Bacmeister, J. T.: Widespread solid particle formation by mountain waves in the Arctic stratosphere, J. Geophys. Res., 104(D1), 1827–1836, doi:10.1029/1998JD100033, 1999.

Carslaw, K. S., Kettleborough, J. A., Northway, M. J., et al.: A vortex-scale simulation of the growth and sedimentation of large nitric acid hydrate particles, J. Geophys. Res., 107(D20), 8300, doi:10.1029/2001JD000467, 2002.

Cziczo, D. J., Thomson, D. S., and Murphy, D. M.: Ablation, Flux and Atmospheric Impications Inferred from Stratospheric Aerosol, Science, 291, 1772–1775, 2001.

Cziczo, D. J., Murphy, D. M., Hudson, P. K., and Thomson, D. S.: Single particle measurements of the chemical composition of cirrus ice residue during Crystal Face, J. Geophys. Res., 109(D4210), 4517, doi:10.1029/2003JD004032, 2004.

Davies, S., Mann, G., Carslaw, K. S., et al.: 3-D microphysical model studies of Arctic denitrification: comparison with observations, Atmos. Chem. Phys. Discuss., 5, 347–393, 2005, **SRef-ID: 1680-7375/acpd/2005-5-347**.

Deshler, T., Larsen, N., Weisser, C., et al.: Large nitric acid particles at the top of an Arctic stratospheric cloud, J. Geophys. Res., 108(D16), 4517, doi:10.1029/2003JD003479, 2003.

Dörnbrack, A., Leutbecher, M., Kivi, R., and Kyrö, E.: Mountain-wave induced record low stratospheric temperatures above northern Scandinavia, Tellus, 51A, 951–963, 1999.

Drdla, K., Schoeberl, M. R., and Browell, E. V.: J. Geophys. Res., 108(D5), 8312, doi:10.1029/2001JD000782, 2003.

Dhaniyala, S., McKinney, K. A., and Wennberg, P. O.: Lee-wave clouds and denitrification of the polar stratosphere, Geophys. Res. Lett., 29(9), doi:10.1029/2001GL013900, 2002.

Fahey, D., Solomon, S., Kawa, S. R., et al.: Observations of denitrification and dehydration in the polar winter stratosphere, Nature, 344, 321–324, 1990.

Fahey, D. W., Gao, R. S., Carslaw, K. S., et al.: The detection of large HNO_3-containing particles in the winter arctic stratosphere, Science, 291, 1026–1031, 2001.

Fueglistaler, S., Luo, B. P., Voigt, C., et al.: NAT-rock formation by mother clouds: a microphysical model study, Atmos. Chem. Phys., 2, 93–98, 2002, **SRef-ID: 1680-7324/acp/2002-2-93**.

Grooß, J. U., Günther, G., Müller, R., et al.: Simulation of denitrification and ozone losse for the Arctic winter 2002/2003, Atmos. Chem. Phys. Discuss., 4, 8069–8101, 2004, **SRef-ID: 1680-7375/acpd/2004-4-8069**.

Hanson, D. and Mauersberger, K.: Laboratory studies of the nitric acid trihydrate: Implications for the south polar stratosphere, Geophys. Res. Lett., 15, 855–858, 1988.

Hinds, W. C.: Aerosol technology: properties, behaviour, and measurement of airborne particles, 2nd ed., John Wiley & Sons, Inc., New York, 1999.

Hunten, D., Turco, R. P., and Toon, O. B.: Smoke and Dust Particles of Meteoric Origin in the Mesosphere and Stratosphere, J. Atmos. Sci., 37, 6, 1342–1357, 1980.

Knopf, D. A., Koop, T., Luo, B. P., et al.: Homogeneous nucleation of NAD and NAT in liquid stratospheric aerosols: insufficient to explain denitrification, Atmos. Chem. Phys., 2, 207–214, 2002, **SRef-ID: 1680-7324/acp/2002-2-207**.

Koop, T., Biermann, U. M., Raber, W., et al.: Do stratospheric aerosol droplets freeze above the ice frost point?, Geophys. Res. Lett., 22(8), 917–920, doi:10.1029/95GL00814, 1995.

Koop, T., Luo, B. P., Biermann, U., et al.: Freezing of $HNO_3/H_2SO_4/H_2O$ Solutions at Stratospheric Temperatures: Nucleation Statistics and Experiments, J. Phys. Chem. A, 101, 1117–1133, 1997.

Koop, T., Luo, B. P., Tsias, A., and Peter, T.: Water activity as the determinant for homogeneous ice nucleation in aqueous solutions, Nature, 406, 611–614, 2000.

Krämer, M. and Afchine, A.: Sampling characteristics of inlets operated at low U/U_0 ratios: new insights from computational fluid dynamics (CFX) modeling, J. Aerosol Sci., 35, 6, 683–694, 2004.

Larsen, N., Knudsen, B., Svendsen, S., et al.: Formation of solid particles in synoptic-scale Arctic PSCs in early winter 2002/2003, Atmos. Chem. Phys., 4, 2001–2013, 2004, **SRef-ID: 1680-7324/acp/2004-4-2001**.

Luo, B., Voigt, C., Füglistaler, S., and Peter, T.: Extreme NAT supersaturations in mountain wave ice PSCs: a clue to NAT formation, J. Geophys. Res., 108(D15), 4441,

doi:10.1029/2002JD003104, 2003.

Mann, G., Davies, S., Carslaw, K., and Chipperfield, M.: Factors controlling Arctic denitrification in cold winters of the 1990s, Atmos. Chem. Phys., 3, 403–416, 2003,
SRef-ID: 1680-7324/acp/2003-3-403.

Mangold, A., Wagner, R., Saathoff, H., Schurath, U., Giesemann, C., Ebert, V., Kraemer, M., and Moehler, O.: Experimental investigation of ice nucleation by different types of aerosols in the aerosol chamber AIDA: implications to microphysics of cirrus clouds, Meteorol. Z., in press, 2005.

Mitev, V., Matthey, R., and Makarov, V.: Miniature backscatter lidar for cloud and aerosol observation from high altitude aircraft, Rec. Res. Devel. Geophys., 4, 207, ISBN: 81-7736-076-0, 2002.

Murphy, D. M., Thomson, D. S., and Mahoney, M. J.: In situ Measurements of Organics, Meteoritic Material, Mercury and Other Elements in Aerosols at 5 to 19 Kilometers, Science, 282, 1664–1667, 1998.

Northway, M. J., Gao, R. S., Popp, P. J., et al.: An analysis of large HNO_3-containing particles sampled in the Arctic stratosphere during the winter of 1999–2000, J. Geophys. Res., 107, 8289, doi:10.1029/2001JD001079, 2002.

Peter, T.: Microphysics and heterogeneous chemistry of polar stratospheric clouds, Ann. Rev. Phys. Chem., 48, 785–822, 1997.

Poole, L. R., Trepte, C. R., Harvey, V. L., et al.: SAGE III observations of Arctic polar stratospheric clouds – December 2002, Geophys. Res. Lett., 30(23), 2216–2220, 2003.

Salcedo, D., Molina, L. T., and Molina, M. J.: Homogeneous Freezing of Concentrated Aqueous Nitric Acid Solutions at Polar Stratospheric Temperatures, J. Phys. Chem., 105, 1433–1439, 2001.

Schreiner, J., Voigt, C., Kohlmann, A., et al.: Chemical analysis of polar stratospheric cloud particles, Science, 283, 968–970, 1999.

Schreiner, J., Voigt, C., Mauersberger, K., et al.: Chemical, microphysical, and optical properties of polar stratospheric clouds, J. Geophys. Res., 108, 8313, doi:10.1029/2001JD000825, 2003.

Schiller, C., Bauer, R., Cairo, F., et al.: Dehydration in the Arctic stratosphere during the SOLVE/THESEO-2000 campaigns, J. Geophys. Res., 107(D20), 8293, doi:10.1029/2001JD000463, 2002.

Schmitt, J.: Aufbau und Erprobung eines in-situ NO/NOy-Mess-Systems am Höhenforschungsflugzeug Geophysica, PhD Thesis, edited by: DLR, D-51170 Köln, ISRN DLR-FB-2003-21, 2004.

Scientific Assessment of ozone depletion, 1998, WMO Report No. 44, Geneva, 1999.

Tabazadeh, A., Djikaev, Y. S., Hamill, P., et al.: Laboratory evidence for surface nucleation of Solid Polar Stratospheric Cloud Particles, J. Phys. Chem. A, 106, 10 238–10 246, 2002.

Thomas, A.: In situ measurements of background aerosol and subvisible cirrus in the tropical tropopause region, J. Geophys. Res., 107(D24), 4763, doi:10.1029/2001JD001385, 2002.

Tolbert, M. and Toon, B.: Solving the PSC mystery, Science, 292, 61–63, 2001.

Toon, O. B., Tabazadeh, A., Browell, E. V., and Jordan, J.: Analysis of lidar observations of Arctic polar stratospheric clouds during January 1989, J. Geophys. Res., 105(16), 20 589–20 615, 2000.

Voigt, C., Schreiner, J., Kohlmann, A., et al.: Nitric Acid Trihydrate (NAT) in Polar Stratospheric Clouds: Science, 290, 1756–1758, 2000a.

Voigt, C., Tsias, S., Dörnbrack, A., et al.: Non-equilibrium compositions of liquid polar stratospheric clouds in gravity waves, Geophys. Res. Lett., 27, 3873–3876, 2000b.

Voigt, C., Larsen, N., Deshler, T., et al.: In situ mountain-wave polar stratospheric cloud measurements: Implications for nitric acid trihydrate formation, J. Geophys. Res., 108(D5), doi:10.1029/2001JD001185, 2003.

Wirth, V., Tsias, A., Dörnbrack, A., Weiß, V., Carslaw, K. S., Leutbecher, M., Renger, W., Volkert, H., and Peter, T.: Model-guided Lagrangian observation and simulation of mountain polar stratospheric clouds, J. Geophys. Res., 104(D19), 23 971–23 982, doi:10.1029/1998JD900095, 1999.

Worsnop, D. R., Fox, L. E., Zahniser, M. S., and Wofsy, S. C.: Vapor pressures of solid hydrates of nitric acid: implications for polar stratospheric clouds, Science, 259, 71–74, 1993.